Mechanisms of flame spread and burnout in large enclosure fires

Vinny Gupta[a,*], Andres F. Osorio[a], José L. Torero[b], Juan P. Hidalgo[a]

[a] *School of Civil Engineering, University of Queensland, St. Lucia Campus, Brisbane 4067, Australia*

[b] *Department of Civil, Environmental & Geomatic Engineering, University College London, London, United Kingdom*

* Corresponding author; E-mail address: v.gupta@uq.edu.au

Keywords: enclosure fires, flame spread, burning rates, full-scale experiments

Abstract

Knowledge of the first principles defining fire behaviour in large enclosures remains limited despite their common use in modern tall buildings. The evolution of a fire in large enclosures can be defined by the relationship between the flame front and burnout velocities (V_S/V_{BO}). The mechanisms governing flame spread and burnout are investigated using four full-scale enclosure fire experiments with high porosity wood cribs with similar enclosure geometries. Flame and burnout fronts position and velocity are estimated using video data. Velocities are affected by the heat feedback from the enclosure and smoke layer to the fuel. The spread velocity shows two regimes, a critical heat flux below which there is no spread ($\dot{q}''_{s,crit}$) and a heat flux that defines the onset of very rapid flame spread ($\dot{q}''_{rs,crit}$). A phenomenological model is developed to help identify the underlying mechanisms controlling the transition between the different spread modes. Both the model and data show that $\dot{q}''_{s,crit}$ is controlled by the fuel's surface temperature ahead of the flame front, and that $\dot{q}''_{s,crit}$ reduces as the surface temperature approximates steady state. The magnitude of $\dot{q}''_{rs,crit}$ is constant and is mainly delivered by the flame heat flux. The dependence of the burnout front velocity to the external radiation is found to be weak.

Nomenclature

A	area
b	stick thickness
C	crib burning constant
h_T	total heat transfer coefficient
L_v	latent heat of vaporisation
m'	mass per unit length
$\dot{m}''_b$	burning rate per unit area
$\dot{m}''_o$	free burning rate per unit area
$\dot{m}''_r$	radiation enhanced burning rate per unit area
$\dot{q}''_e$	external radiant heat flux
$\dot{q}''_f$	radiative heat flux from the flame front
$\dot{q}''_{ig,crit}$	critical heat flux for ignition
$\dot{q}''_{rs,crit}$	critical heat flux for rapid flame spread
$\dot{q}''_{s,crit}$	critical heat flux for flame spread
R	ratio of exposed wood to floor areas
T	temperature
t	time
V_{BO}	burnout front velocity
V_S	flame front velocity
W	fuel bed width

$\widetilde{k\rho c}$	apparent thermal inertia of the solid
Δt_{BO}	characteristic burnout time
Δt_{ig}	characteristic ignition delay time

Greek symbols

ϕ'	inverse opening factor
ρ	solid density
δ	characteristic length

Subscripts

0	ambient
F	floor
ig	ignition
h	heated
L	burning
O	opening
s	surface
t	top surface

1. Introduction

The underpinning knowledge of enclosure fire dynamics rests upon a vast body of research developed from the 1950s to the 1970s focused on small enclosures with restricted openings [1]. Thomas and Heselden [2] experimentally showed a clear distinction between two regimes, a ventilation-controlled regime and a momentum-controlled regime. It was shown that in the ventilation-controlled regime, the fire dynamics of small enclosures are defined by the opening area, and the enclosure acts as a well-stirred reactor. The burning rate and temperature are determined by oxygen transport into the compartment. In the momentum-controlled regime, the burning process is governed by the residence time. In this case temperatures and burning rates are controlled by complex transport processes. In both regimes, total consumption of the fuel is controlled by the quantity and nature of the fuel [3], and the enclosure's thermal feedback to the fuel. In the ventilation-controlled regime, heat exchange between the enclosure and the fuel is described by a simple total heat transfer coefficient, but in the momentum-controlled regime, quantification of the heat transfer to the fuel is highly dependent on the geometry of the enclosure, and thus no solution was ever proposed [1].

Large open-plan enclosures largely fall outside the ventilation-controlled regime [1]. A review of the limited set of full-scale enclosure fire experiments by Stern-Gottfried *et al*. [4], shows significant spatial and temporal distribution of temperatures in medium to large enclosures. Experiments in large enclosures showed that the fire dynamics are defined by the velocity of a propagating flame front (V_S), and the velocity of a propagating burnout front (V_{BO}) [5]. Based on the relationship between the flame front and burnout front (V_S/V_{BO}), three fire spread modes were identified [6]:

- Mode 1: a fully-developed fire where $V_S/V_{BO} \to \infty$
- Mode 2: a growing fire where $V_S/V_{BO} > 1$
- Mode 3: a steady moving fire where $V_S/V_{BO} \approx 1$

Existing theories for flame spread in thermally-thick fuels show that flame radiation, external radiation, fuel material properties and fuel arrangement control flame spread and the burning rates [7]. Environmental variables such as oxygen concentration and flow conditions also influence flame

propagation and burning behaviour. However, the specific mechanisms by which environmental variables interact with the propagation and burning behaviour in large enclosures remain unknown.

This study explores the mechanisms controlling the propagation of the flame and burnout fronts using four full-scale enclosure fire experiments across three separate experimental campaigns with a similarity in fuel and compartment geometry. Fires were initiated on one side of the enclosure and allowed to propagate along a wood crib freely. The velocity and the external heat flux at both the flame and burnout fronts were measured. A phenomenological model is developed to study the role of the ratio of the flame front and burnout front velocities.

2. Methodology

2.1 Enclosure and fuel characteristics

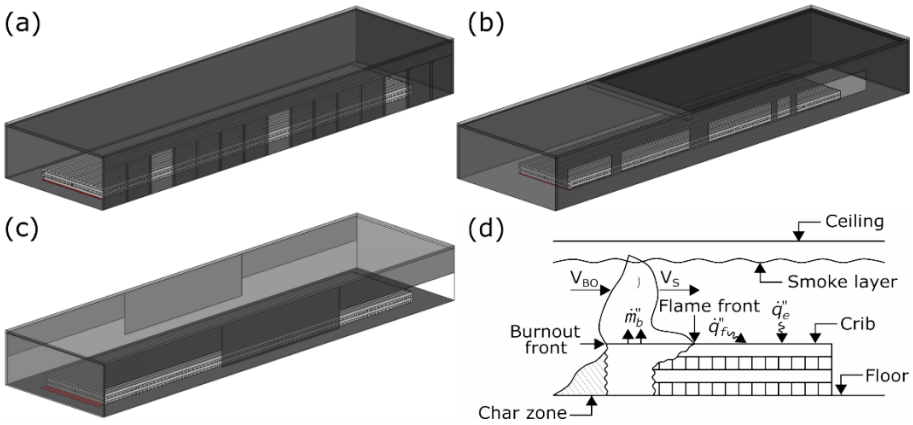

Fig. 1. Experimental set-up used in each experiment. (a) is used for Test 1 (all openings unrestricted) and Test 2 (three openings). (b) is used for Test 3 (the shaded area on the ceiling shows the combustible cork). (c) is used for Test 4. (d) shows the physical parameters common to each experiment.

Four full-scale experiments with similar fuel conditions and enclosure characteristics are considered for this study. These include two wood crib tests from the Edinburgh Tall Building Fire Tests (ETFT) programme [8], the Malveira Fire Test (MFT) [6], and the Guttasjön Fire Test (GFT) [9] referred as Test 1 through 4, respectively. Key instrumentation includes video cameras used to determine the position of the flame and burnout fronts, and thin-skin calorimeters (TSCs) [10] used to quantify the external radiation onto the fuel. Details of the set-up are provided in Fig. *1* and Table 1, with additional descriptions found in [6,8,9]. However, the data from Test 1, 2 and 4 have not been

reported before. Test 1 and Test 2 were conducted in the same enclosure with two inverse opening factors ($\phi' = A_T/A_O\sqrt{H_O}$) of ϕ' = 4.1 $m^{-0.5}$ (Test 1), and ϕ' = 23.3 $m^{-0.5}$ (Test 2).

Table 1.

Summary of enclosure and fuel characteristics for each experiment

Experiment Name	ETFT 1 [8]	ETFT 2 [8]	MFT[a] [6]	GFT [9]
Test No.	1	2	3	4
Enclosure Characteristics				
Geometry, L x W x H (m)	18 x 5 x 2	18 x 5 x 2	21 x 4.7 x 2.85	18 x 6 x 3
A_O (m^2)	16.5	3.3	16.12	61.8
ϕ' ($m^{-0.5}$)	4.1	23.3	4.6	2.3
Fuel Characteristics				
Wood species	Pinus Sylvestris	Pinus Sylvestris	Pinus Pinaster	Picea Abies
Crib geometry, L x W (m)	16 x 3	16 x 3	16 x 2.4	15.2 x 2.5
# layers (-)	4	4	3.5	4
Total weight (kg)	2496	2496	2306	1698
Stick thickness (cm)	5	5	5	4.5
Crib Porosity [11] (cm)	0.20	0.20	0.25	0.18
Exposed surface area (m^2)	288	288	228	228
Moisture Content (%)	11 ± 0.4	11.5 ± 0.7	19 ± 6	15.8 ± 2

[a] a deep beam soffit and combustible cork lining is positioned at 8.5m (from the ignition of the fuel bed) in length along the ceiling.

For Tests 1 and 2, three cameras were positioned outside and facing the compartment opening (spaced every 4m), and six cameras were mounted on the back wall of the compartment (spaced every 3m) also facing the compartment opening. Fifteen TSCs (spaced every 1.2m) were mounted at each side of the fuel on the floor. Test 3 used five cameras and eight TSCs (spaced every 1.5m) on both sides of the fuel on the floor. In Test 4, six cameras were positioned on one side (spaced every 3m), with eleven TSCs (spaced every 1.5m) mounted both sides of the fuel, near the floor.

2.2 Measurement of flame and burnout fronts

Frames from each video are extracted at different times to describe the progression of the flame and burnout fronts. A luminance threshold is used to define the leading edge of the flame, while the burnout front position is determined based on the sharp reduction in luminance at the flame trailing. The instantaneous velocity of the flame and burnout fronts are determined using a second-order central differencing scheme for the first derivative of the front positions. Quantification of the external radiation measured by the TSCs along the fuel bed follows the procedure detailed by Hidalgo *et al*. [10]. Heat fluxes at each length coordinate on both sides of the fuel bed are averaged. The external heat flux at the flame front is an instantaneous quantity, quantified by linearly interpolating the two closest TSCs to the flame front position. The external heat flux at the burnout front is determined in each timestep by averaging the heat flux imposed at the burnout front position from the ignition time to burnout time.

2.3 Controlling parameters of flame spread and burnout in an enclosure

Equation (1) shows that the flame spread rate of a thermally thick fuel is controlled by the heat flux of the flame front, $\dot{q}_{\mathrm{f}}''$ acting upon a heated length, δ_{h}, and a surface temperature T_s of the solid upon arrival of the flame front [12].

$$V_{\mathrm{S}} = \frac{\delta_{\mathrm{h}}}{\Delta t_{\mathrm{ig}}} = \frac{4\,(\dot{q}_{\mathrm{f}}'')^2 \delta_{\mathrm{h}}}{\pi\left(\widetilde{k\rho c}\right)\left(T_{\mathrm{ig}} - T_{\mathrm{s}}\right)^2} \qquad (1)$$

The surface temperature of the solid is controlled by the external radiation, $\dot{q}_e''$ from the smoke layer and enclosure and the thermal properties. The temperature evolves in time as given by [7]:

$$T_{\mathrm{s}} = T_0 + \frac{\dot{q}_{\mathrm{e}}''}{h_{\mathrm{T}}}\left[1 - e^{\left(\frac{h_{\mathrm{T}}^2}{k\rho c}\right)t}\,\mathrm{erfc}\left(\frac{h_{\mathrm{T}}}{(k\rho c)^{0.5}}\,t^{0.5}\right)\right] \qquad (2)$$

Equation (2) shows that $\dot{q}_{\mathrm{e}}''$ controls the preheating of the solid ahead of the flame front. Comparison of the characteristic timescales shows that the magnitude of the timescale to heat the gas-phase with $\dot{q}_{\mathrm{f}}''$ is considerably smaller than pre-heating the solid-phase with $\dot{q}_{\mathrm{e}}''$ [7]. Thus, sudden rises in

the flame spread rate are associated with significant increases in $\dot{q}_{\mathrm{f}}''$, while the slow acceleration is related to the preheating of the solid ahead of the flame front by $\dot{q}_{\mathrm{e}}''$.

To evaluate the ratio of the flame spread and burnout front velocities, Eq. (2) is modified to formulate the solution for the ignition delay time (Δt_{ig}) on the basis that the heat flux determines the surface temperature, T_{s}. This temperature is raised from ambient conditions, T_0, to T_{s} when heated by the external heat flux, $\dot{q}_{\mathrm{e}}''$ to steady-state. The flame then raises the temperature from T_{s} to the ignition temperature, T_{ig}. In this case, Quintiere's model [12] is altered to approximate this condition and Δt_{ig} is defined by the time to raise the surface temperature from T_{s} to T_{ig}. Using this assumption, the ignition delay time is given as:

$$\Delta t_{\mathrm{ig}} = \frac{\pi \widetilde{k\rho c}\left(\dot{q}_{\mathrm{ig,crit}}'' - \dot{q}_{\mathrm{e}}''\right)^2}{4h_{\mathrm{T}}^2 \dot{q}_{\mathrm{f}}''^2} \qquad (3)$$

The characteristic burnout duration along a one-dimensional length is given as a function of the mass per unit length, fuel width and burning rate per unit area:

$$\Delta t_{\mathrm{BO}} = m'W/\dot{m}_{\mathrm{b}}'' A_s \qquad (4)$$

For a wood crib, $\dot{m}_{\mathrm{b}}''$ in Eq. (4) is a function of the free crib burning rate, $\dot{m}_{\mathrm{o}}''$, and the radiation enhanced burning rate, $\dot{m}_{\mathrm{r}}''$ [13]:

$$\dot{m}_{\mathrm{b}}'' = \dot{m}_{\mathrm{o}}'' + \dot{m}_{\mathrm{r}}'' \qquad (5)$$

For high porosity wood cribs, $\dot{m}_{\mathrm{o}}''$ is evaluated as a function of the exposed surface area of sticks, A_{S}, and is evaluated using Block's model [14]:

$$\dot{m}_{\mathrm{o}}/A_{\mathrm{s}} = Cb^{-0.5} \qquad (6)$$

$\dot{m}_{\mathrm{r}}''$ over the top exposed surface of a wood crib, $A_{\mathrm{s,t}}$, is approximated as [13]:

$$\dot{m}_{\mathrm{r}}/A_{\mathrm{s,t}} = \dot{q}_{\mathrm{e}}''/L_{\mathrm{v}} \qquad (7)$$

Both Eq. (6) and Eq. (7) show the burning rate as a function of the exposed surface area and exposed top surface area of the crib (A_{s} and $A_{\mathrm{s,t}}$). Based on the crib geometry, the exposed surface area is given by the floor area and ratio of exposed wood to floor areas:

$$A_{\mathrm{s}} = R_1 A_F = R_1 W \delta_{\mathrm{L}} \quad (8)$$

$$A_{\mathrm{s,t}} = R_2 A_{\mathrm{F}} = R_2 W \delta_{\mathrm{L}} \quad (9)$$

Combining Eq. (4-9) and considering that m' over a small length (i.e. b) can be expressed as $m' = \rho b^2$, the characteristic burnout time is a function of the crib geometry and $\dot{q}''_{\mathrm{e}}$:

$$\Delta t_{\mathrm{BO}} = \frac{\rho b^2}{C b^{-0.5} R_1 \delta_{\mathrm{L}} + \frac{\dot{q}''_{\mathrm{e}}}{L_v} R_2 \delta_{\mathrm{L}}} \quad (10)$$

Thus, combining Eq. (3) and Eq. (10) delivers the ratio of the flame and burnout front velocities for a wood crib as a function of two mechanisms: $\dot{q}''_{\mathrm{e}}$ and $\dot{q}''_{\mathrm{f}}$.

$$\frac{V_{\mathrm{S}}}{V_{\mathrm{BO}}} = \frac{\Delta t_{\mathrm{BO}}}{\Delta t_{\mathrm{ig}}} = \frac{4\rho b^2 \dot{q}''^2_{\mathrm{f}} h_{\mathrm{T}}^2}{\pi \widetilde{k\rho c} \left(\dot{q}''_{\mathrm{ig,crit}} - \dot{q}''_{\mathrm{e}}\right)^2 \left(C b^{-0.5} R_1 \delta_{\mathrm{L}} + \frac{\dot{q}''_{\mathrm{e}}}{L_v} R_2 \delta_{\mathrm{L}}\right)} \quad (11)$$

Equation (11) will be used to evaluate the ratio of flame spread to burnout for the four wood crib fuels from the experiments.

3. Results and Discussion

3.1 Evolution of flame and burnout fronts

Figure 2 shows the flame and burnout front locations and the calculated instantaneous velocities for each test. The errors of the instantaneous velocities are evaluated using the frames per second, timestep, pixel resolution and instantaneous velocity, following Bhattacharjee *et al.*'s approach [15]. Average flame front velocity errors are low, ranging within ±1.5-10% except when V_s increases rapidly. Burnout front velocity errors range within ±1.5-3%, showing small fluctuations.

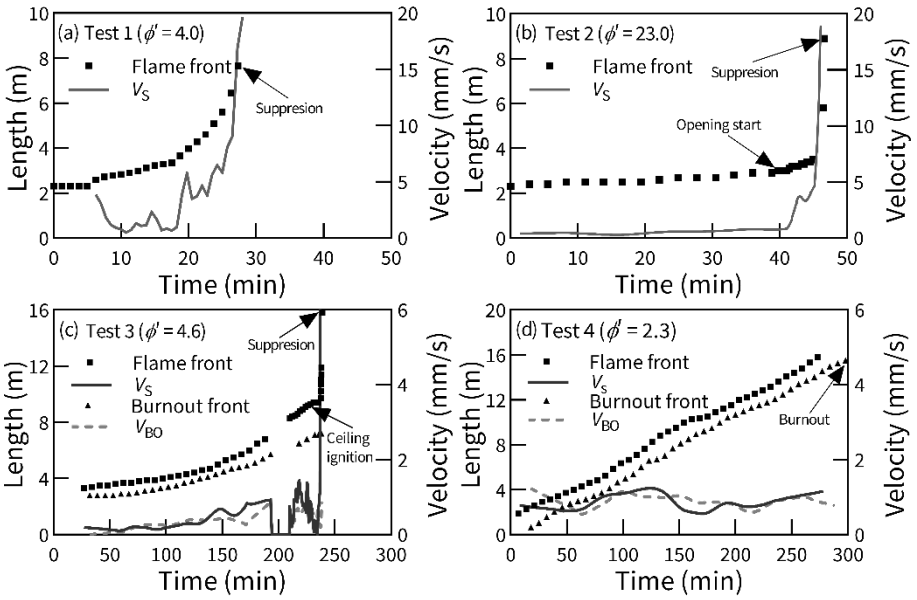

Fig. 2. Position and instantaneous velocity of the flame and burnout front for each test.

In Test 1 (Fig. 2a), a shallow smoke layer forms over the enclosure after ignition. Flame spread accelerates weakly, indicating that mild pre-heating of the fuel bed controls the flame front acceleration. After 20 minutes, the flame spread starts accelerating faster until 24 minutes, when the flame spread velocity spikes. The duration of the test is too short for a moving burnout front to form. Thus, two fire spread modes are identified in terms of V_S/V_{BO}; Mode 2 ($V_S/V_{BO} > 1$) from 0-24 minutes, with a short transition to Mode 1 ($V_S/V_{BO} \to \infty$) from 24 minutes onwards until suppression.

Test 2 (Fig. 2b) uses the same enclosure, but the ventilation is restricted (ϕ' = 23 $m^{-0.5}$). The ignition zone is located 2 metres behind the first opening. The reduction of ventilation has a major influence on the flame spread rate resulting in slow flame front propagation for the first 39 minutes despite a denser and thicker smoke layer when compared to Test 1. As the flame front reaches the opening, both the flame spread rate and intensity increase. Flames continue to spread until 45 minutes, at which point the virgin fuel bed ahead of the flame front shows signs of pyrolysis, followed by a rapid spike of the propagation rate. The increase in the flame intensity as the fire front approaches the opening indicates that the combustion zone is under-ventilated, thus the flame heat fluxes are low and spread rates are initially small. Once again, the test is short, and a moving burnout front does not form. The same two fire spread modes are identified; Mode 2 ($V_S/V_{BO} > 1$) from 0 to 45 minutes, and a transition to Mode 1 ($V_S/V_{BO} \to \infty$) afterwards.

Test 3 (Fig. 2c) shows a similar behaviour as Tests 1 and 2, but in this case, the slow spread lasts for 227 minutes allowing for a burnout front to be formed [6]. This test includes a combustible cork ceiling that ignites at 227 minutes. The flame spread accelerates slightly as the flame front approaches the beam in the centre of the enclosure until 237 minutes, at which point the flame spread spikes. The flaming along the ceiling accelerates the descent of the smoke layer. Three fire spread modes are identified; Mode 3 ($V_S/V_{BO} \approx 1$) from 0-152 minutes, Mode 2 ($V_S/V_{BO} > 1$), from 152-237 minutes, followed by a final transition to Mode 1 ($V_S/V_{BO} \to \infty$).

No such transitions are identified in Test 4 (Fig. 2d), where relatively constant flame and burnout front velocities are found, ranging from 0.8-1.2 mm/s and corresponding to Mode 3 ($V_S/V_{BO} \approx 1$). Due to the large openings, a smoke layer does not form, so pre-heating far from the flame is minimal.

3.2 Evaluation of enclosure thermal feedback to the propagation velocity of the flame and burnout fronts

Figure 3 shows the variation of the velocity of the flame and burnout fronts as a function of the measured external heat flux. The data points are an ensemble of at least 10 data points, and the error bars show the 95% confidence interval for the velocity. Figure 3 also shows a critical heat flux for flame spread ($\dot{q}''_{s,crit}$), i.e. the minimum heat flux induced by the compartment that is measured at the arrival of the flame front and necessary to sustain surface flame spread based on the concept of Quintiere and Harkleroad [16].

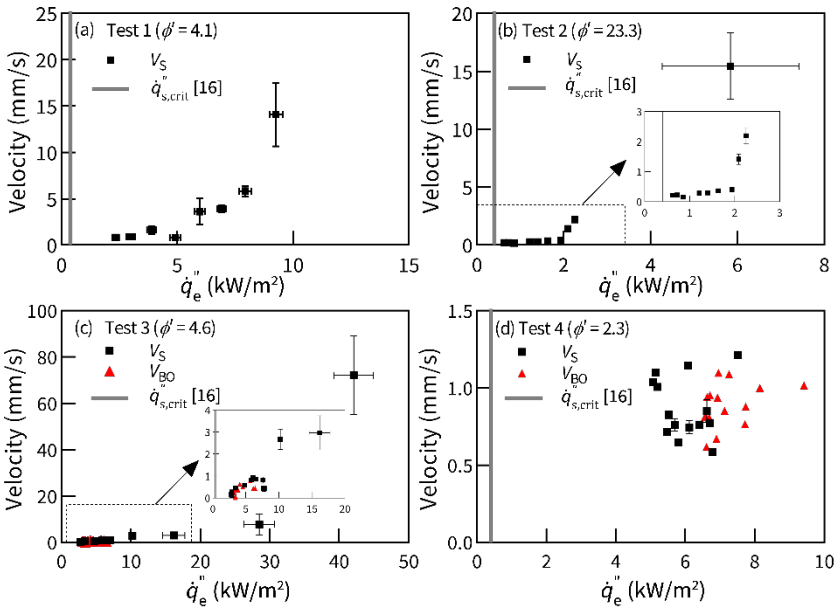

Fig. 3. Comparison of the flame and burnout front velocity and external heat flux to both fronts for each test. The vertical line is the steady-state critical heat flux for flame spread, $\dot{q}''_{s,crit}$ obtained by Quintiere [16], using the LIFT apparatus.

Across all tests, a higher external heat flux corresponds to a higher flame front velocity. The same is not found for the burnout front velocity which ranges from 0.2-1.2 mm/s irrespective of heat flux (Test 3 and 4), indicating that external radiation from the enclosure does not significantly affect the wood crib burning rate.

The critical heat flux for flame spread ($\dot{q}''_{\mathrm{s,crit}}$) as measured at the arrival of the flame front varies across all tests, with $\dot{q}''_{\mathrm{s,crit}}$ being 2.3 kW/m^2 in Test 1, 0.6 kW/m^2 in Test 2, 2.8 kW/m^2 in Test 3, and 5.0 kW/m^2 in Test 4.The variation of $\dot{q}''_{\mathrm{s,crit}}$ is linked to the pre-heating of the fuel ahead of the flame front. Lower values of $\dot{q}''_{\mathrm{s,crit}}$ correlate with greater pre-heating (Eq. (1)) and the potential attainment of thermal equilibrium between gas and solid phases (Eq. (11)). Given that $\dot{q}''_{\mathrm{s,crit}}$ relates to Eq. (1), it is expected that short-lived changes in the external heat flux will show only a minor effect on $\dot{q}''_{\mathrm{s,crit}}$. This explains the mild effect of the flaming ceiling in Test 3 on the magnitude of $\dot{q}''_{\mathrm{s,crit}}$, as there is only a 100-second pre-heating time under these conditions. In Test 2, pre-heating occurs for over 40 minutes, thus $\dot{q}''_{\mathrm{s,crit}}$ was significantly lower. Two limiting conditions are therefore established based on the capacity of the pre-heated solid to reach a steady-state surface temperature:

1. $\dot{q}''_{\mathrm{s,crit}}$ is controlled by the pre-heating ahead of the flame front, $\dot{q}''_{\mathrm{e}}(x)$ with the limiting case being Test 2, where $\dot{q}''_{\mathrm{s,crit}}$ approaches the steady-state value obtained by Quintiere (Fig. 3b) [16]. Thus, if the intensity of $\dot{q}''_{\mathrm{e}}(x)$ is significant and the pre-heating duration of the solid increases, then $\dot{q}''_{\mathrm{s,crit}}$ decreases.
2. The other limit is Test 4, where the enclosure heat losses are sufficiently high that there is no preheating of the solid and therefore $\dot{q}''_{\mathrm{s,crit}}$ is largest.

In Test 3, a transition from Mode 3 ($V_{\mathrm{S}}/V_{\mathrm{BO}} \approx 1$) to Mode 2 ($V_{\mathrm{S}}/V_{\mathrm{BO}} > 1$) is obtained, however, no transitions occur in Test 4; despite similar spread and burnout velocities in Mode 1, suggesting that a threshold exists for a transition from Mode 3 to Mode 2. The key difference in both tests is the size of the openings (smaller in Test 3), and the presence of the soffit beam in Test 3 that allows local smoke build-up around the beam [6]. Therefore, the pre-heating duration of the solid ahead of the flame front is longer and enables a transition to slightly faster flame spread rates.

The threshold for rapid flame spread ($V_{\mathrm{S}}/V_{\mathrm{BO}} \to \infty$ or Mode 1) can be defined using a critical heat flux, $\dot{q}''_{\mathrm{rs,crit}}$, which under testing conditions is referred to as the critical heat flux for piloted ignition, $\dot{q}''_{\mathrm{ig,crit}}$. The value of $\dot{q}''_{\mathrm{rs,crit}}$ can be obtained from the data as the highest heat flux before the attainment of rapid flame spread. Fig. 3 shows a large variation of $\dot{q}''_{\mathrm{rs,crit}}$ across all tests. In Test 1 and 2, $\dot{q}''_{\mathrm{rs,crit}}$ occurs at 9.3 kW/m^2 and 5.8kW/m^2 respectively, while in Test 3, $\dot{q}''_{\mathrm{rs,crit}}$ occurs between 10.2-28.5 kW/m^2. Rapid flame spread does not occur in Test 4, where the heat fluxes at the flame front remain below 7.5 kW/m^2.

The role of the flame heat flux is evaluated using the ratio of $V_{\mathrm{S}}/V_{\mathrm{BO}}$ in Eq. (11). The flame spread and burnout process occur over a characteristic length, δ which is assumed as the stick thickness, b. The flame heat flux, $\dot{q}''_{\mathrm{f}}$ is found by fitting Eq. (11) to the experimental data for $V_{\mathrm{S}}/V_{\mathrm{BO}}$ at heat fluxes below $\dot{q}''_{\mathrm{rs,crit}}$, shown in Fig. 4. The model in Eq. (11) assumes that the solid surface temperature approximates steady state. The model assumptions no longer apply when $\dot{q}''_{\mathrm{rs,crit}}$ is attained as physically this parameter is transient and the contribution of the flame is modified such that solid surface temperature ahead of the flame front can no longer pre-heat to a steady state.

The apparent thermal inertia, $\widetilde{k\rho c}$ and $\dot{q}''_{\mathrm{ig,crit}}$, are determined through Cone Calorimeter testing of the sticks from Test 1 and 2. Input parameters are shown in Table 2. Fuel properties specific to the tests are extracted from Table 1. The total heat transfer coefficient, h_{T} is calculated assuming that $T_{\mathrm{s}} = T_{\mathrm{ig}}$, the empirical crib coefficient, C is obtained from Block [14], and the latent heat of vaporisation, L_{v} is specified as per data by Quintiere and McCaffrey [3].

Table 2
Model Parameters

$\dot{q}''_{\mathrm{f}}$[a] (kW/m^2)	4.4, 12.3, 2.8, 2.5
$\widetilde{k\rho c}$ (kW^2/m^{4}K^{4}s)	0.468
$\dot{q}''_{\mathrm{ig,crit}}$ (kW/m^2)	10.5
h_{T} (W/m^{2}K)	37.5
C (g/s.cm$^{1.5}$)	0.00103
R_1[b] (-)	6, 5.67
R_2[b] (-)	0.67, 0.75
L_{v} (kJ/g)	1.8

[a] $\dot{q}''_{\mathrm{f}}$ from Test 1 to 4 respectively

[b] Constant for 3.5- and 4-layer cribs respectively

Despite the duration of Test 1 and 2 being too short to attain a propagating burnout front, the burnout velocity was assumed based on observations of Test 3 and Test 4, where the burnout front propagates at a fixed rate early in both experiments such that $V_{\mathrm{S}}/V_{\mathrm{BO}} \approx 1$. The burnout front velocity for Test 1 and 2 was assumed to be equivalent to the flame spread rate for the first 3 minutes of each experiment once the contribution from the ignition tray stopped such that V_{BO} is 0.7 mm/s and 0.25 mm/s respectively.

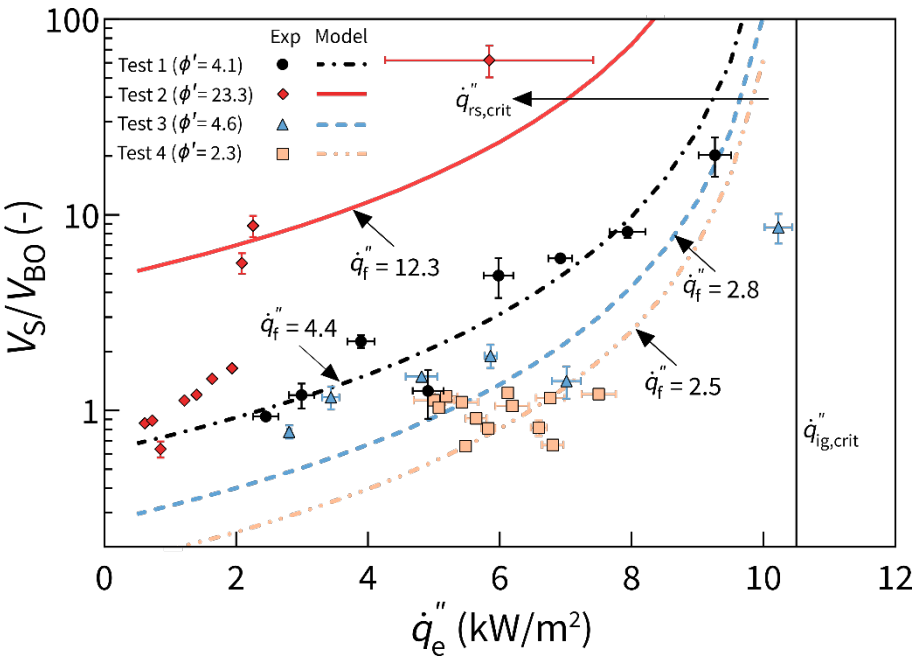

Fig. 4 Phenomenological model results compared to the experimental data for each test. The range of $\dot{q}''_{s,crit}$ is shown for reference.

Figure 4 shows the quantification of Eq. (11) together with the experimental data. The fitted value for $\dot{q}''_f$ is presented for all tests showing that the model follows the data for $\dot{q}''_e$ before the attainment of $\dot{q}''_{rs,crit}$. Once a steady flame contribution is established, the model demonstrates that the characteristic timescales of solid-phase heating control the ratio of spread to burnout rates through a larger magnitude of $\dot{q}''_f$. Figure 4 demonstrates that the ventilation conditions have a direct impact on $\dot{q}''_f$. For Test 1, the data correlates well for $\dot{q}''_f \approx 4.4$ kW/m^2. For Test 2, a significant jump is observed from 5.3-12.3 kW/m^2 when ventilation is changed dramatically. Test 4, being very well ventilated, shows the lowest values for $\dot{q}''_f$ as the pre-heating ahead of the flame is sufficiently low and rapid flame spread is not attained. Test 3 shows a smaller flame contribution, with the data correlates well for $\dot{q}''_f \approx 2.8$ kW/m^2, which is slightly higher than Test 4. The transition of modes occurs as $\dot{q}''_e$ rises beyond $\dot{q}''_{ig,crit}$ due to the enhanced thermal feedback induced from the flaming ceiling. The model diverges from the data at $\dot{q}''_{rs,crit}$ as the steady state assumption of the solid no longer applies.

4. Conclusions

In this study, the mechanisms controlling the flame spread and burnout of a fuel bed within an enclosure are studied using four large-scale enclosure fire experiments with similarity in the geometry and wood crib fuel bed. The analysis shows a strong coupling of the flame front velocity to the heat flux supplied by the smoke layer and enclosure; however, a weak relationship is found in the case of the burnout front velocity, which plateaus at 1 mm/s. The experimental data shows that conditions within the enclosure (low ventilation, combustible ceilings) can induce rapid propagation of the flame front through different heat pathways. Changes in the ventilation can lead to an increase in the heat flux directly supplied by the flame suddenly. The addition of additional thermal feedback into the fuel from a flaming ceiling is sufficient to overcome the small contribution of the heat flux supplied from the flame. The phenomenological model indicates that the ratio of V_{S} and V_{BO} correlates well with estimated heat fluxes. The critical heat flux for flame spread, $\dot{q}''_{\mathrm{s,crit}}$ varies across each test and is found to be controlled by the capacity of the solid ahead of the flame front to pre-heat. As the solid approaches a steady-state surface temperature, the flame contribution increases and less heat from the enclosure is required to continue spreading. The closer the solid is pre-heated to the ignition temperature, the greater the magnitude of the spread. These results demonstrate that flame spread and burnout within an enclosure are controlled by the energy balance at the fuel surface. Two components of this energy balance appear; the pre-heating component corresponding to slow evolution and the flame related component corresponding to sudden changes. Based on this analysis, Mode 3 ($V_{\mathrm{S}}/V_{\mathrm{BO}} \approx 1$) occurs if the enclosure heat losses are sufficiently high such that the pre-heating ahead of the flame front is low, therefore $\dot{q}''_{\mathrm{s,crit}}$ is large, and the contribution of $\dot{q}''_{\mathrm{f}}$ is small. Transitions to Mode 2 ($V_{\mathrm{S}}/V_{\mathrm{BO}} > 1$) occur if preheating timescale of the solid by $\dot{q}''_{\mathrm{e}}$ is sufficient enough to reduce $\dot{q}''_{\mathrm{s,crit}}$. Finally, the onset of a transition to Mode 1 ($V_{\mathrm{S}}/V_{\mathrm{BO}} \to \infty$) is defined by $\dot{q}''_{\mathrm{rs,crit}}$, which is delivered by the magnitude of $\dot{q}''_{\mathrm{f}}$ on the basis that the pre-heating timescales of the solid ahead of the flame front are sufficiently long to approximate steady state. If steady state is not attained, $\dot{q}''_{\mathrm{e}}$ must be significantly increased beyond $\dot{q}''_{\mathrm{ig,crit}}$ by means of an additional heat source such as a flaming ceiling.

Acknowledgements

This work is supported by the EPSRC (Grant No. EP/J001937/1) and RFCS (Grant No. 754198). The authors thank Tristan Goode for prior contributions to this work and are grateful to David Lange, Johan Sjöström, Fredrick Kahl, Emil Hallberg, Alastair Temple, Adam Cowlard, Cecilia Abecassis-Empis and others for their role in the experiments.

5. References

[1] J.L. Torero, A.H. Majdalani, A.E. Cecilia, A. Cowlard, Revisiting the compartment fire, Fire Saf. Sci. 11 (2014) 28–45. doi:10.3801/IAFSS.FSS.11-28.

[2] P.H. Thomas, A.J.M. Heselden, Fully Developed Fires in Single Compartments, (1972).

[3] T.Z. Harmathy, The role of thermal feedback in compartment fires, Fire Technol. 11 (1975) 48–54. doi:10.1007/BF02590002.

[4] J. Stern-Gottfried, G. Rein, L.A. Bisby, J.L. Torero, Experimental review of the homogeneous temperature assumption in post-flashover compartment fires, Fire Saf. J. 45 (2010) 249–261. doi:10.1016/j.firesaf.2010.03.007.

[5] V. Gupta, J.P. Hidalgo, A. Cowlard, C. Abecassis-Empis, A.H. Majdalani, C. Maluk, J.L. Torero, Ventilation effects on the thermal characteristics of fire spread modes in open-plan compartment fires, Fire Saf. J. (in Press. (2020).

[6] J.P. Hidalgo, T. Goode, V. Gupta, A. Cowlard, C. Abecassis-Empis, J. Maclean, A.I. Bartlett, C. Maluk, J.M. Montalvá, A.F. Osorio, J.L. Torero, The Malveira fire test: Full-scale demonstration of fire modes in open-plan compartments, Fire Saf. J. 108 (2019) 102827. doi:10.1016/j.firesaf.2019.102827.

[7] J.G. Quintiere, Fundamentals of Fire Phenomena, 1st Editio, Wiley, 2006.

[8] J.P. Hidalgo, A. Cowlard, C. Abecassis-Empis, C. Maluk, A.H. Majdalani, S. Kahrmann, R. Hilditch, M. Krajcovic, J.L. Torero, An experimental study of full-scale open floor plan enclosure fires, Fire Saf. J. 89 (2017) 22–40. doi:10.1016/j.firesaf.2017.02.002.

[9] J. Sjostrom, E. Hallberg, F. Kahl, A. Temple, S. Welch, X. Dai, V. Gupta, D. Lange, J. Hidalgo, Characterization of TRAvelling FIRes in large compartments, 2019.

[10] J.P. Hidalgo, C. Maluk, A. Cowlard, C. Abecassis-Empis, M. Krajcovic, J.L.J.L. Torero, A Thin Skin Calorimeter (TSC) for quantifying irradiation during large-scale fire testing, Int. J. Therm. Sci. 112 (2017) 383–394. doi:10.1016/j.ijthermalsci.2016.10.013.

[11] G. Heskestad, Modeling of enclosure fires, Symp. Combust. 14 (1973) 1021–1030. doi:10.1016/S0082-0784(73)80092-X.

[12] J.G. Quintiere, A theoretical basis for flammability properties, Fire Mater. 30 (2006) 175–214. doi:10.1002/fam.905.

[13] J.G. Quintiere, B.J. McCaffrey, The burning of wood and plastic cribs in an enclosure, Washtington DC, 1980.

[14] J.A. Block, A theoretical and experimental study of nonpropagating free-burning fires, Symp. Combust. 13 (1971) 971–978. doi:10.1016/S0082-0784(71)80097-8.

[15] S. Bhattacharjee, L. Carmignani, G. Celniker, B. Rhoades, Measurement of instantaneous flame spread rate over solid fuels using image analysis, Fire Saf. J. 91 (2017) 123–129. doi:10.1016/j.firesaf.2017.03.039.

[16] J.G. Quintiere, M. Harkleroad, New Concepts for Measuring Flame Spread Properties, Gaithersburg, 1984.